MAKÜFEBED

Mehmet Akif Ersoy Üniversitesi Fen Bilimleri Enstitüsü Dergisi
The Journal of Graduate School of Natural and Applied Sciences of Mehmet Akif Ersoy University
Volume: 17 Issue: 1 - 2026 | Cilt: 17 Sayı 1 - 2026

Strain-Induced Electronic and Optical Properties of Rb_2O Monolayer: Bandgap Modulation and Semiconductor to Metal Transition

Tek katmanlı Rb_2O'nun Gerinime Bağlı Elektronik ve Optik Özellikleri: Bant Aralığı Modülasyonu ve Yarıiletken Metal Geçişi

Yakup BORAN[1*]

[1] Sakarya University of Applied Sciences, Faculty of Technology, Department of Engineering Fundamental Sciences, Sakarya, Türkiye

Article Info

Research Article

DOI:10.29048/makufebed.1943578

Corresponding Author

Yakup BORAN

Email: yakupboran@subu.edu.tr

Article History

Received: 04.05.2026

Revised: 06.06.2026

Accepted: 08.06.2026

Available Online: 30.06.2026

To Cite

Boran, Y. (2026). Strain-induced Electronic and optical properties of rb2o monolayer: bandgap modulation and semiconductor to metal transition. *The Journal of Graduate School of Natural and Applied Sciences of Mehmet Akif Ersoy University, 17*(1), 39–47. https://doi.org/10.29048/makufebed.1943578

ABSTRACT: In this study, the comprehensive first-principles investigation of the structural, electronic, and biaxial strain-dependent properties of the two-dimensional (2D) Rubidium oxide (Rb_2O) monolayer is presented using density functional theory (DFT) within the WIEN2k framework. The optimized lattice constant is found to be approximately 4.25 Å. At zero strain, the Rb_2O monolayer exhibits a semiconducting behavior with a band gap of about 1.38 eV. The modulation of electronic properties under biaxial strain is systematically analyzed in the range of −6% to +6% with the increment of 2%. The results reveal a strong strain dependence of the band gap. Under tensile strain, the band gap increases and reaches approximately 1.58 eV at +6% strain. In contrast, under compressive strain, the bandgap decreases sharply and vanishes around −5.5% strain, indicating a semiconductor to metal transition. Furthermore, the optical response, characterized by the absorption coefficient and optical conductivity, shows a pronounced dependence on the biaxial strain, with significant enhancement and spectral shifts observed in the ultraviolet (UV) region. These findings demonstrate that the Rb_2O monolayer possesses highly tunable electronic and optical properties, highlighting its potential for strain-engineered nanoelectronic and UV-range optoelectronic applications.

Keywords: 2D materials, Rb2O monolayer, density functional theory, WIEN2k, biaxial strain, bandgap modulation

ÖZ: Bu çalışmada, iki boyutlu (2B) tek katmanlı rubidyum oksitin (Rb_2O) yapısal, elektronik ve çift eksenli gerinime bağlı özelliklerinin ilk prensiplerle incelenmesi, WIEN2k programında yoğunluk fonksiyonel teorisi (DFT) kullanılarak kapsamlı bir şekilde ele alınmıştır. Optimize edilmiş örgü sabiti yaklaşık 4,25 Å olarak bulunmuştur. Sıfır gerinim altında Rb_2O, tek katmanlı yapısı ile yaklaşık 1,38 eV bant aralığına sahip yarı iletken davranış sergilemektedir. Elektronik özelliklerin çift eksenli gerinim altındaki değişimi −%6 ile +%6 aralığında %2'lik artışla sistematik olarak analiz edilmiştir. Elde edilen sonuçlar, bant aralığının gerinime güçlü bir şekilde bağlı olduğunu göstermektedir. Çekme gerinimi altında bant aralığı artarak +%6 gerinimde yaklaşık 1,58 eV değerine ulaşmaktadır. Buna karşılık, basma gerinimi altında bant aralığı hızla azalmakta ve yaklaşık −%5,5 gerinim civarında ortadan kalkarak yarıiletken-metal geçişine işaret etmektedir. Ayrıca, soğurma katsayısı ve optik iletkenlik ile karakterize edilen optik etkinin de gerinime belirgin şekilde bağlı olduğu, özellikle morötesi (UV) bölgede önemli artışlar ve spektral kaymaların meydana geldiği gözlemlenmiştir. Bu bulgular, Rb_2O tek katmanlı yapısının yüksek derecede ayarlanabilir elektronik ve optik özelliklere sahip olduğunu ortaya koymakta olup, gerinim mühendisliği temelli nanoelektronik ve UV bölgesinde çalışan optoelektronik uygulamalar için umut verici bir aday olduğunu göstermektedir.

Anahtar Kelimeler: 2B malzemeler, tek katmanlı Rb2O, yoğunluk fonksiyonel teorisi, WIEN2k, iki eksenli gerinim, band aralığı modülasyonu

Burdur Mehmet Akif Ersoy University Press
E ISSN: 1309-2243

1. INTRODUCTION

Low-dimensional materials, particularly two-dimensional (2D) monolayer materials, are known to exhibit distinct properties when compared to their bulk forms. Since the discovery of 2D graphene (Novoselov et al., 2004), research into 2D materials has grown rapidly because of their excellent properties and their potential use in new electronic and optical applications (Molina-Sánchez and Wirtz, 2011; Zhang et al., 2017a). Following this discovery, a diverse range of 2D materials have been widely studied both theoretically and experimentally, such as silicene (Vogt et al., 2012), phosphorene (Zhang et al., 2018), hexagonal boron nitride (h-BN) (Zhang et al., 2017b), transition metal dichalcogenides (TMDCs) (Wang et al., 2012), and MXenes (Fu et al., 2021). Their tunable electronic structure and enhanced surface-to-volume ratio make them particularly promising for next-generation functional devices.

Among emerging 2D materials, alkali metal–based compounds have recently attracted significant interest for their unique electronic, optical, and mechanical properties. In particular, di-alkali metal oxides and chalcogenides (A_2X, where A = Li, Na, K, Rb and X = O, S, Se, Te) have been theoretically predicted to exhibit diverse electronic behaviors ranging from semiconducting to metallic states. Previous studies on Li_2O (Roondhe et al., 2021), Na_2O (Rueshwin and Eithiraj, 2025), and K_2O (Lien et al., 2022) monolayers have revealed promising characteristics for optoelectronic applications. These findings highlight the potential of alkali-based 2D oxides as versatile materials for device engineering. Within this family, Rubidium oxide (Rb_2O) remains relatively unexplored compared to other alkali-based 2D oxides, despite belonging to the same group. A recent first-principles study on Rb_2O monolayers systematically investigated its intrinsic structural, electronic, optical, and thermoelectric properties using PBE-GGA within WIEN2k, confirming its dynamical stability and promising optical and thermoelectric performance for photovoltaic and waste recovery applications (Rueshwin and Eithiraj, 2024).

Despite these comprehensive insights, the influence of external perturbations, particularly mechanical strain, on the electronic structure and optical response of the Rb_2O monolayer within a more accurate mBJ potential has not been systematically explored. Furthermore, unlike previous PBE-GGA-based investigations, the present work employs the mBJ potential to provide a more reliable description of the electronic structure under biaxial strain. In addition, the strain-dependent evolution of optical properties is analyzed to further elucidate the optoelectronic potential of the Rb_2O monolayer. Strain engineering has been shown to induce significant electronic transitions in 2D materials, including semiconductor-to-metal transitions under sufficient compressive strain, highlighting its effectiveness as a powerful tool for modulating band structures. Although the Rb_2O monolayer has not yet been experimentally synthesized and remains a theoretically predicted material, first-principles calculations provide an effective approach to explore its fundamental properties and guide future experimental efforts. In this work, the effects of both tensile and compressive biaxial strain on the electronic and optical properties of the Rb_2O monolayer have been investigated. Particular attention is given to the strain-dependent evolution of the band structure and the corresponding changes in optical properties, including the dielectric function, optical conductivity, and absorption coefficient. This study aims to provide deeper insight into strain-driven property modulation in alkali-based 2D oxides and to assess the potential of Rb_2O for tunable nanoelectronic and optoelectronic applications.

2. MATERIAL AND METHODS

2.1. Computational Details

First-principles calculations were performed for the Rb_2O monolayer within the framework of density functional theory (DFT) using the full-potential linearized augmented plane wave (FP-LAPW) method as implemented in the WIEN2k package (Blaha et al., 2020). The exchange–correlation potential was described using the generalized gradient approximation (GGA) in the Perdew–Burke–Ernzerhof (PBE) form (Perdew et al., 1997). For a more accurate description of the electronic structure, especially the band gap, the modified Becke–Johnson (mBJ) potential was employed (Tran and Blaha, 2009). The Brillouin zone was sampled with a Monkhorst-Pack k-point mesh of 10×10×1 for the self-consistent (SCF) calculations. The muffin-tin radii (RMT) were chosen as 2.5 a.u. for Rb and 1.8 a.u. for O atoms. The dimensionless plane-wave cutoff parameter was chosen as $R_{MT}K_{max}$ = 7, where R_{MT} is the smallest muffin-tin radius and K_{max} is the magnitude of the largest reciprocal lattice vector. The maximum Fourier expansion of the charge density was set to G_{max} = 12. The core–valence separation energy was fixed at −6 Ry. The convergence criteria were set to 10^{-4} Ry for total energy and 10^{-3} e for charge. The internal atomic positions were fully relaxed until the forces on each atom were below 1 mRy/Bohr. To model the two-dimensional nature of the Rb_2O monolayer, a vacuum layer of 15 Å was introduced along the out-of-plane direction to eliminate interactions between periodic images.

2.2. Strain Application

The effect of strain on the structural and electronic properties was investigated by applying biaxial strain. The strain (ε) was defined as:

$$\varepsilon = (a - a_0)/a_0 \quad (1)$$

where a and a_0 represent the strained and equilibrium lattice constants, respectively, negative and positive strain values correspond to compressive and tensile strains. The

strain was varied in the range of −6% to +6%. To ensure structural stability under applied strain, full atomic relaxation was performed for each strain configuration while keeping the lattice deformation fixed. This approach allows the accurate evaluation of strain-induced modifications in both electronic structure and optical properties. The selected strain range is sufficient to capture both the elastic response and possible electronic phase transitions of the system.

2.3. Optical Calculations

Optical properties were calculated within the DFT framework using the OPTIC module of WIEN2k. For these calculations, a denser k-point mesh of 20×20×1 was used to ensure accurate evaluation of optical spectra. The real (ε_1) and imaginary (ε_2) parts of the dielectric function provide essential information regarding the optical response and interband electronic transitions of the system. The total dielectric function is defined as (Sun et al., 2004),

$$\varepsilon(\omega) = \varepsilon_1(\omega) + i\varepsilon_2(\omega) \quad (2)$$

where $\varepsilon_1(\omega)$ represents the polarizability of the material, while $\varepsilon_2(\omega)$ corresponds to the optical absorption. $\varepsilon_2(\omega)$ was computed from the momentum matrix elements, and $\varepsilon_1(\omega)$ was obtained via the Kramers–Kronig relations. Based on the calculated complex dielectric function, the optical conductivity ($\sigma(\omega)$) and absorption coefficient ($\alpha(\omega)$) were derived. $\alpha(\omega)$ and $\sigma(\omega)$ are expressed as (John and Padmavathi, 2016; Saha et al., 2000):

$$\alpha(\omega) = \frac{\sqrt{2}\omega}{c}\left[\sqrt{\varepsilon_1{}^2(\omega) + \varepsilon_2{}^2(\omega)} - \varepsilon_1(\omega)\right]^{1/2} \quad (3)$$

$$\sigma(\omega) = \frac{\omega}{4\pi}\varepsilon_2(\omega) \quad (4)$$

These calculated optical parameters enable a detailed analysis of strain-dependent optical behavior.

3. RESULT AND DISCUSSION

3.1. Structural Optimization

To investigate the structural optimization of the Rb_2O monolayer, the PBE-GGA exchange correlation functionals were employed in WIEN2k. The Rb_2O monolayer crystallizes in a trigonal structure with 164 (P-3m1) (Rueshwin and Eithiraj, 2024). The structural optimization was performed by calculating the total energy as a function of the lattice constant. A series of self-consistent calculations was carried out for different lattice parameters to determine the equilibrium configuration. Figure 1 shows the optimized unit cell and the 3x3x1 supercell of the Rb_2O monolayer in top view, along with the total energy–lattice parameter curve. The curve exhibits a typical parabolic dependence on the lattice constant, indicating the stability of the system. The equilibrium lattice parameter was obtained.

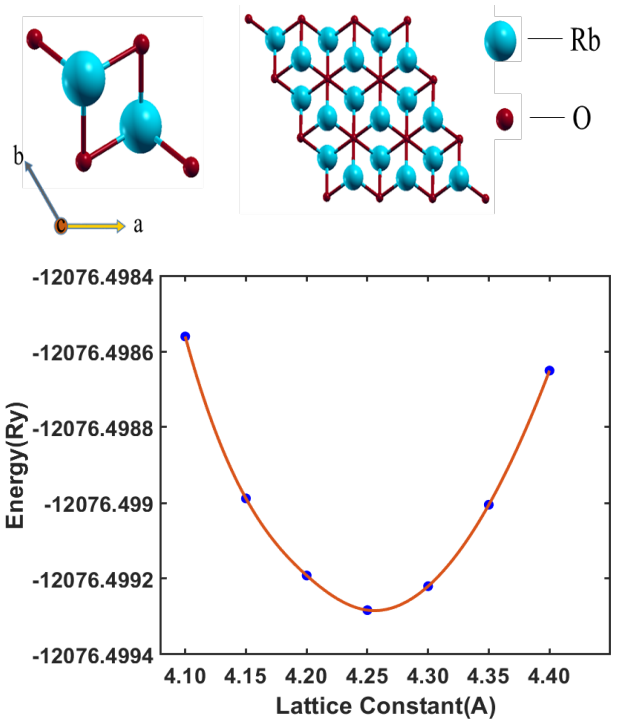

Figure 1. Optimized atomic structure of Rb_2O monolayer: unit cell and 3x3x1 supercell in top view (top), and lattice parameter optimization curve using PBE-GGA functional (bottom)

from the minimum of the fitted curve and was found to be approximately a ≈ 4.25 Å. This optimized lattice constant was subsequently used for all further electronic and optical property calculations. The smooth variation of the energy curve confirms the reliability and convergence of the computational approach. The obtained equilibrium lattice constant is slightly lower than the previously reported value of ~4.43 Å (Rueshwin and Eithiraj, 2024). Such a deviation can be attributed to differences in computational approaches, including the treatment of internal atomic coordinates and relaxation schemes.

3.2. Mechanical Properties

To evaluate the mechanical response of the Rb_2O monolayer, the in-plane stiffness (C_{2D}) was calculated from the strain–energy relationship. A series of total energy calculations was performed under biaxial strain in the range of −6% to +6%, and the resulting energy values were fitted with a second-order polynomial, as shown in Figure 2. The in-plane stiffness was determined using the following equation (Wei and Peng, 2014):

$$C_{2D} = \frac{1}{A_0}\frac{d^2E}{d\varepsilon^2} \quad (5)$$

where A_o is the equilibrium area of the unit cell, and ε is the applied strain. The second derivative was extracted from the quadratic fitting coefficient, considering the conversion of strain from percentage to fractional form. The smooth parabolic behavior of the strain–energy curve

(Figure 2) confirms the mechanical stability of the structure within the investigated strain range. The calculated in-plane stiffness of the Rb_2O monolayer is found to be approximately 37 N/m. For comparison, graphene exhibits an exceptionally high stiffness of ~340 N/m (Lee et al., 2008), while a monolayer.

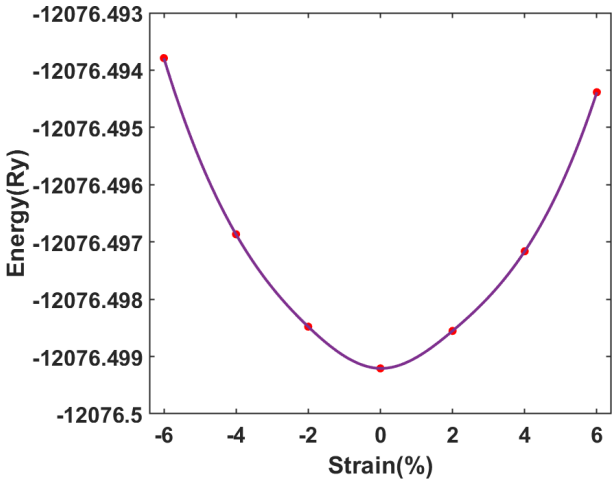

Figure 2. Variation of the total energy as a function of applied biaxial strain in the Rb2O monolayer. The solid line shows a quadratic fit to the calculated data.

MoS_2 has a stiffness of ~120–130 N/m (Bertolazzi et al., 2011). These comparisons indicate that the Rb_2O monolayer is significantly more flexible than the widely studied 2D materials. The applied biaxial strain range (−6% to +6%) falls well within the typical limits reported for 2D materials. Graphene can sustain strains up to ~20%, while MoS_2 can tolerate strains of approximately 10–15% before mechanical failure. Therefore, the chosen strain range is physically reasonable and ensures structural stability. The relatively low in-plane stiffness of the Rb_2O monolayer (~37 N/m) suggests enhanced mechanical flexibility, which is advantageous for strain engineering applications. This mechanical softness facilitates efficient modulation of electronic and optical properties under external strain.

3.3. Electronic Properties

The electronic band structure of the Rb_2O monolayer was calculated along the high-symmetry paths Γ–M–K–Γ using both the PBE-GGA and the mBJ approaches, as shown in Figure 3. The results confirm the semiconducting nature of the Rb_2O monolayer. As depicted in Figure 3, the system exhibits an indirect bandgap, with the valence band maximum (VBM) located near the M point and the conduction band minimum (CBM) near the Γ point. The band gaps obtained using the PBE-GGA and mBJ functionals are 0.31 eV and 1.39 eV, respectively. The underestimated bandgap in the PBE-GGA results is consistent with the well-known limitation of standard GGA functionals.

In contrast, the mBJ potential yields a significantly improved bandgap, providing a more reliable description of the electronic structure. The obtained band gaps with PBE-GGA and mBJ are in good agreement with previously reported theoretical studies (0.52 eV and 1.52 eV) for Rb_2O monolayers, confirming the validity of the present computational approach since the mBJ approach describes the electronic structure more accurately than PBE-GGA. All electronic and optical property calculations were carried out using the mBJ approach.

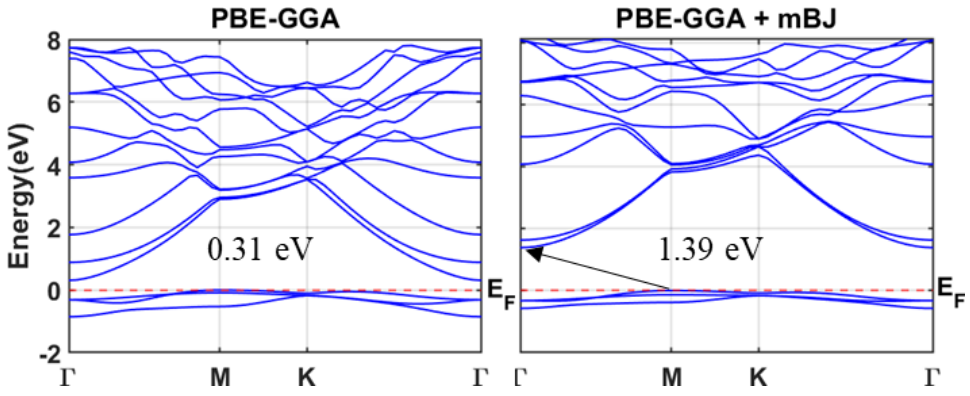

Figure 3. Electronic band structures of the Rb_2O monolayer calculated using PBE-GGA and PBE-GGA + mBJ functionals

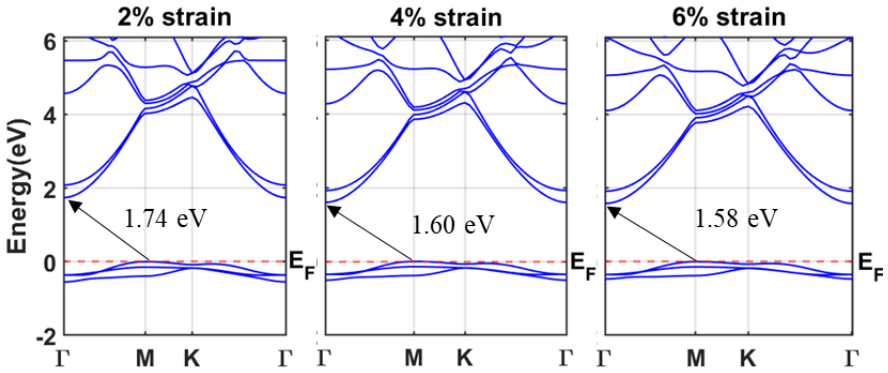

Figure 4. Electronic band structures of the Rb_2O monolayer under tensile biaxial strain calculated using mBJ functionals

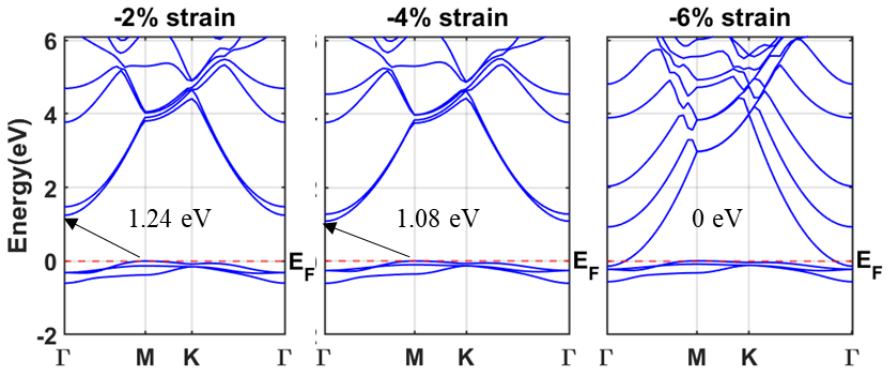

Figure 5. Electronic band structures of the Rb_2O monolayer under compressive biaxial strain calculated using mBJ functionals

To investigate the strain-dependent electronic properties of the Rb_2O monolayer, biaxial tensile and compressive strains were applied, and the corresponding band structures, calculated using the mBJ potential, are shown in Figures 4 and 5. The results reveal that the electronic structure of Rb_2O is highly sensitive to external strain. Under tensile strain, the bandgap gradually increases from its unstrained value, reaching approximately 1.74 eV at 2% strain, followed by a slight reduction at higher strain levels (1.60 eV at 4% and 1.58 eV at 6%). This behavior indicates a tunable semiconducting response under stretching. In contrast, compressive strain leads to a continuous decrease in the bandgap, reducing it to 1.24 eV at −2% strain and further to 1.08 eV at −4% strain. Notably, at −6% compressive strain, the bandgap closes entirely, indicating a semiconductor-to-metal transition. The evolution of the band gap under strain reveals a clear asymmetry between tensile and compressive regimes, as presented in Figure 6. While tensile strain induces an initial widening of the band gap followed by a slight reduction, compressive strain drives a rapid decrease toward zero. The band gap approaches zero around −5.5% strain, marking the onset of the metallic phase. This transition can be attributed to the relative shifts of the valence and conduction bands toward the Fermi level, ultimately leading to band overlap. Such behavior originates from strain-induced modifications in bond lengths and bond angles, which alter orbital interactions and consequently affect the electronic band structure. A similar trend has been reported in other two-dimensional materials, confirming the effectiveness of strain engineering as a powerful approach for tuning electronic properties (Ju et al., 2015). Overall, this pronounced sensitivity highlights that compressive strain is a more effective mechanism for modulating the electronic properties of the Rb_2O monolayer, suggesting its potential for strain-controlled nanoelectronic and optoelectronic applications.

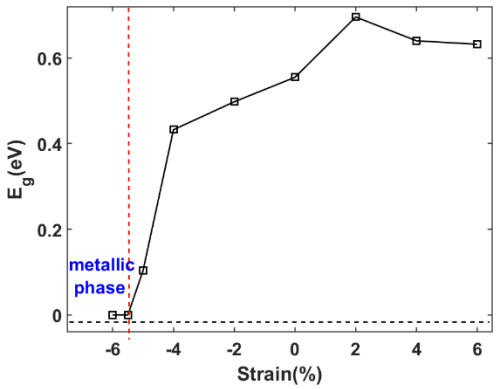

Figure 6. The bandgap of the Rb_2O monolayer obtained with mBJ as a function of strain

To gain further insight into the strain-dependent electronic properties, the total and partial density of states (TDOS and PDOS) of the Rb_2O monolayer were analyzed under +6% and –6% strain and compared with the unstrained case, as shown in Figure 7. In the unstrained case, a clear bandgap is observed, with a complete absence of electronic states at the Fermi level, confirming the semiconducting nature of the system. The valence band is primarily dominated by O states, while Rb contributions are mainly located in the conduction band, indicating a clear separation of orbital contributions. Under tensile strain (+6%), the overall DOS profile remains largely similar, with only slight shifts in the peak positions near the band edges. The bandgap is

preserved, consistent with the semiconducting behavior observed in the band structure analysis. In contrast, under compressive strain (−6%), a significant modification in the electronic structure is observed. The bandgap completely vanishes, and a finite density of states appears at the Fermi level, indicating a transition from semiconductor to metallic behavior. This transition originates from the overlap between the valence and conduction bands, triggered by the reduction in interatomic distances under compressive strain.

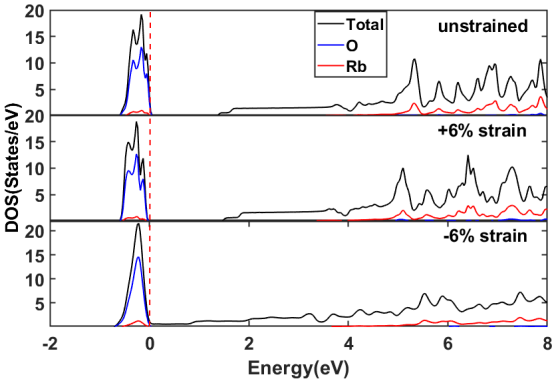

Figure 7. Total and partial density of states (TDOS and PDOS) of the Rb_2O monolayer, calculated with the mBJ functional: unstrained (top), +6% strain (middle), and –6% strain (bottom)

3.4. Optical Properties

In addition to the electronic structure analysis, the optical properties of the Rb_2O monolayer under various biaxial strain cases were also evaluated. The frequency-dependent dielectric function, optical conductivity, and absorption coefficient were calculated and are presented in Figures 8 and 9. Figure 8 illustrates the real $\varepsilon_1(\omega)$ and imaginary $\varepsilon_2(\omega)$ parts of the dielectric function for the unstrained, +6% tensile, and −5% compressive strain conditions within mBJ functionals for the photon energy up to ~14 eV. The static dielectric constant $\varepsilon_1(0)$ is found to be 1.45 for the unstrained structure, slightly decreases to 1.41 under tensile strain, and increases to 1.81 under compressive strain, indicating enhanced polarization under compression. The maximum value of $\varepsilon_1(\omega)$ shifts depending on the applied strain, with the compressive strain case exhibiting the highest peak (1.96 at 0.45 eV), suggesting stronger low-energy optical response. In contrast, tensile strain slightly reduces the peak magnitude and shifts it toward higher photon energies. The imaginary part $\varepsilon_2(\omega)$ shows negligible values below the band gap region, confirming the semiconducting nature of the system. A pronounced increase is observed once the photon energy exceeds the band gap, corresponding to the onset of interband electronic transitions. The peak positions of $\varepsilon_2(\omega)$ exhibit noticeable strain dependence, indicating that biaxial strain effectively modulates the optical transition energies between valence and conduction bands.

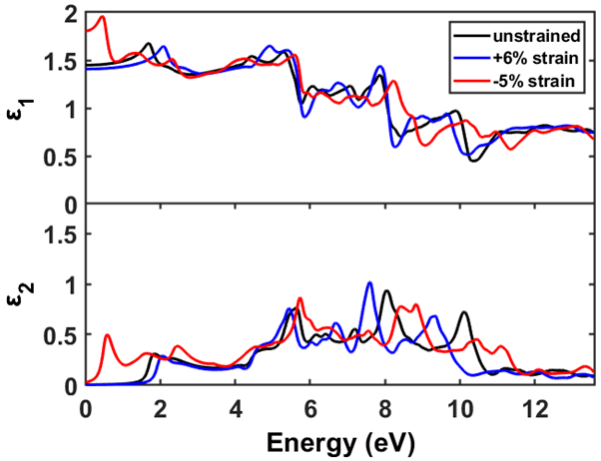

Figure 8. The calculated real $\varepsilon_1(\omega)$ and imaginary $\varepsilon_2(\omega)$ part of the dielectric constant for the Rb_2O monolayer within the mBJ functional for unstrained, +6% strain, and –5% strain

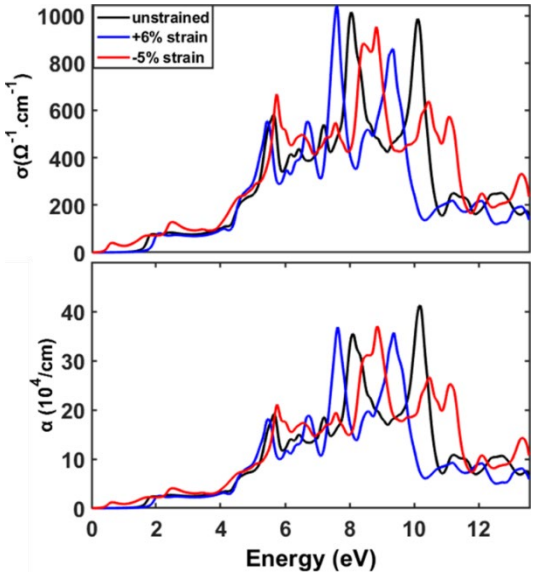

Figure 9. The calculated optical absorption coefficient $\alpha(\omega)$ and optical conductivity $\sigma(\omega)$ of the Rb_2O monolayer within the mBJ functional for unstrained, +6% strain, and –5% strain

The absorption coefficient $\alpha(\omega)$ and the optical conductivity $\sigma(\omega)$, as shown in Figure 9, exhibit closely correlated trends, both remaining negligible below the bandgap threshold and increasing rapidly once photon energies exceed the absorption edge. A pronounced strain dependence is observed in both $\alpha(\omega)$ and $\sigma(\omega)$. Under tensile strain (+6%), a slight shift of the spectral peaks toward higher energies is observed, which can be attributed to the bandgap widening and reduced electronic overlap. On the other hand, compressive strain (–6%) leads to enhanced peak intensities and a shift toward lower energies. This trend is consistent with bandgap narrowing and enhanced orbital hybridization as interatomic distances decrease. These changes are consistent with strain-induced modifications in the bandgap and electronic structure. The prominent peaks in the $\sigma(\omega)$ spectra closely match those observed in $\varepsilon_2(\omega)$, confirming that interband

transitions primarily govern the optical conductivity. Furthermore, both $\alpha(\omega)$ and $\sigma(\omega)$ reach significant values in the ultraviolet (UV) region (~4–12 eV), indicating strong light-matter interaction and suggesting the potential of the Rb_2O monolayer for UV optoelectronic applications. These results highlight the sensitivity of the optical transitions in the Rb_2O monolayer to structural deformations, demonstrating its potential for strain-modulated optoelectronic applications.

Table 1 summarizes the static dielectric constants $\varepsilon_1(0)$, as well as the maximum and minimum values of $\varepsilon_1(\omega)$ along with their corresponding photon energies under different strains. $\varepsilon_1(0)$ slightly decreases under tensile strain (+6%), while it increases noticeably under compressive strain (–5%). The results clearly demonstrate that strain has a pronounced effect on the optical properties of the Rb_2O monolayer. In particular, compressive strain enhances polarization and optical response, while tensile strain slightly suppresses them. These findings indicate that strain engineering provides an effective route for tuning the optical behavior of Rb_2O for potential applications in optoelectronic devices.

Table 1. The static, maximum, and minimum values of the calculated real part of the dielectric function for unstrained (0%), tensile (+6%), and compressive (–5%) strain. Corresponding photon energies are shown in parentheses

Strain	$\varepsilon_1(0)$	max $\varepsilon_1(\omega)$	E (eV)	min $\varepsilon_1(\omega)$	E (eV)
0%	1.45	1.68	1.70	0.447	10.35
+6%	1.41	1.64	2.08	0.513	10.22
–5%	1.81	1.96	0.45	0.570	11.33

Figure 10 presents the calculated refractive index spectra of the Rb_2O monolayer under different biaxial strain conditions. The static refractive index and the overall spectral profile are found to be sensitive to the applied strain. In particular, compressive strain leads to a noticeable increase in the low-energy refractive index, reflecting the enhanced electronic polarizability associated with the narrowed bandgap. Conversely, tensile strain slightly lowers the refractive index and shifts several spectral features toward higher photon energies, consistent with the widening of the bandgap. These results suggest that biaxial strain provides an effective means of tuning the optical propagation characteristics of the Rb_2O monolayer, which could be beneficial for future optoelectronic and photonic applications.

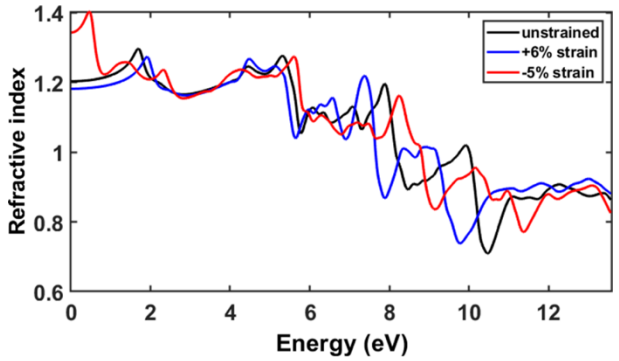

Figure 10. The calculated refractive index of the Rb_2O monolayer within the mBJ functional for unstrained, +6% strain, and –5% strain

The calculated reflectivity spectra under various strain conditions are illustrated in Figure 11. The optical reflectivity of the Rb_2O monolayer exhibits a clear dependence on the applied biaxial strain, particularly within the ultraviolet region where the strongest interband transitions occur. Compressive strain increases the reflectivity and shifts the dominant spectral features toward lower photon energies, whereas tensile strain generally produces the opposite effect. This behavior originates from the strain-induced modification of the electronic band structure and the corresponding redistribution of allowed optical transitions. The ability to manipulate the reflectivity response through external strain further demonstrates the potential of the Rb_2O monolayer as a tunable material for strain-controlled optoelectronic devices.

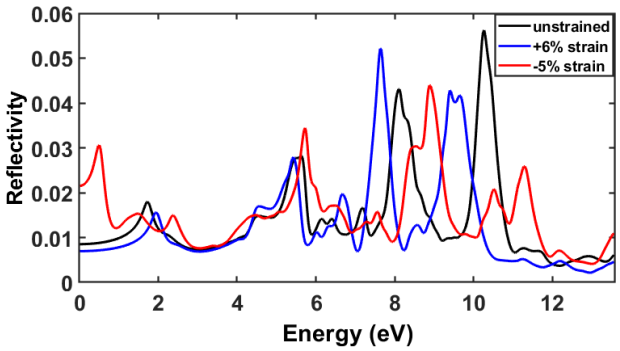

Figure 11. The calculated reflectivity spectra of the Rb_2O monolayer within the mBJ functional for unstrained, +6% strain, and –5% strain

4. CONCLUSION

This study demonstrates the influence of biaxial strain on the electronic and optical properties of the Rb_2O monolayer using a first-principles method in the WIEN2k framework. The results reveal that the material maintains its semiconducting nature under tensile strain, while the compressive strain can change the fundamental semiconductor nature of the system; compressive strain plays a dominant role in modifying the electronic structure. A key finding is the strain-induced bandgap modulation, resulting in a semiconductor to metal transition at around –5.5% compressive strain. This transition is due to

enhanced orbital interactions under compression. The optical properties are found to be strongly correlated with these electronic changes. In the semiconducting regime, the optical spectra exhibit clear shifts. The tensile strain causes a slight shift toward higher photon energies while compressive strain leads to a shift toward lower photon energies, accompanied by enhanced peak intensities. Overall, these findings highlight that biaxial strain not only modifies the bandgap but also effectively controls the optical response of the Rb_2O monolayer. The combination of strain-driven electronic phase transitions and tunable optical behavior suggests that this material could be a good candidate for future applications in optoelectronics and switching technologies.

Author Contributions

Yakup BORAN: (a) Original Idea, (b) Study Design, Methodology, (c) Literature Review, (g) Data Analysis, Interpretation, (h) Writing Text, (i) Critical Review

Declaration of Ethical Code

In this study, we affirm that all the necessary rules under the "Regulation on Scientific Research and Publication Ethics in Higher Education Institutions" have been adhered to, and none of the actions mentioned under the title "Actions Contrary to Scientific Research and Publication Ethics" in the mentioned regulation have been conducted.

Conflict of Interest

The author declares no conflict of interest.

REFERENCES

Bertolazzi, S., Brivio, J., & Kis, A. (2011). Stretching and Breaking of Ultrathin MoS_2. *ACS Nano*, *5*(12), 9703-9709. https://doi.org/10.1021/nn203879f

Blaha, P., Schwarz, K., Tran, F., Laskowski, R., Madsen, G. K. H., & Marks, L. D. (2020). WIEN2k: An APW+lo program for calculating the properties of solids. *The Journal of Chemical Physics*, *152*(7), 074101. https://doi.org/10.1063/1.5143061

Fu, B., Sun, J., Wang, C., Shang, C., Xu, L., Li, J., & Zhang, H. (2021). MXenes: Synthesis, Optical Properties, and Applications in Ultrafast Photonics. *Small*, *17*(11), 2006054. https://doi.org/10.1002/smll.202006054

John, R., & Padmavathi, S. (2016). Ab Initio Calculations on Structural, Electronic and Optical Properties of ZnO in Wurtzite Phase. *Crystal Structure Theory and Applications*, *05*, 24-41. https://doi.org/10.4236/csta.2016.52003

Ju, W., Li, T., Wang, H., Yong, Y., & Sun, J. (2015). Strain-induced semiconductor to metal transition in few-layer black phosphorus from first principles. *Chemical Physics Letters*, *622*, 109-114. https://doi.org/10.1016/j.cplett.2015.01.038

Lee, C., Wei, X., Kysar, J. W., & Hone, J. (2008). Measurement of the Elastic Properties and Intrinsic Strength of Monolayer Graphene. 321(5887), 385-388. https://doi.org/doi:10.1126/science.1157996

Lien, V. T. K., Van On, V., Guerrero-Sanchez, J., Rivas-Silva, J. F., Cocoletzi, G. H., & Hoat, D. M. (2022). Theoretical prediction of alkali oxide M_2O (M = Na and K) monolayers and formation of their Janus structure. *New Journal of Chemistry*, *46*(36), 17386-17393. https://doi.org/10.1039/D2NJ03118C

Molina-Sánchez, A., & Wirtz, L. (2011). Phonons in single-layer and few-layer MoS_2 and WS_2. *Physical Review B*, *84*(15), 155413. https://doi.org/10.1103/PhysRevB.84.155413

Novoselov, K. S., Geim, A. K., Morozov, S. V., Jiang, D., Zhang, Y., Dubonos, S. V., Grigorieva, I. V., & Firsov, A. A. (2004). Electric Field Effect in Atomically Thin Carbon Films. *Science, 306*(5696), 666-669. https://doi.org/doi:10.1126/science.1102896

Perdew, J. P., Burke, K., & Ernzerhof, M. (1997). Generalized Gradient Approximation Made Simple [Phys. Rev. Lett. 77, 3865 (1996)]. *Physical Review Letters*, *78*(7), 1396-1396. https://doi.org/10.1103/PhysRevLett.78.1396

Roondhe, B., Sanyal, S. P., Jha, P. K., Ahuja, R., Shukla, S., & Saxena, S. (2021). H- and T-Li_2O monolayers: Latest addition to 2D flatlands. *Applied Surface Science*, *556*, 149737. https://doi.org/10.1016/j.apsusc.2021.149737

Rueshwin, S. C. T., & Eithiraj, R. D. (2024). An investigation of the 2D Rb_2O monolayer intrinsic properties from a theoretical perspective using DFT. *Journal of Physics and Chemistry of Solids*, *187*, 111855. https://doi.org/10.1016/j.jpcs.2023.111855

Rueshwin, S. C. T., & Eithiraj, R. D. (2025). Structural, electronic, vibrational, optical and thermoelectric properties of 1T-Na_2O monolayer via MD and DFT study. *Physica Scripta*, *100*(1), 015941. https://doi.org/10.1088/1402-4896/ad97ef

Saha, S., Sinha, T. P., & Mookerjee, A. (2000). Electronic structure, chemical bonding, and optical properties of paraelectric$BaTiO_3$. *Physical Review B*, *62*(13), 8828-8834. https://doi.org/10.1103/PhysRevB.62.8828

Sun, J., Wang, H.-T., Ming, N.-B., He, J., & Tian, Y. (2004). Optical properties of heterodiamond B_2CN using first-principles calculations. *Applied Physics Letters*, *84*(22), 4544-4546. https://doi.org/10.1063/1.1758781

Tran, F., & Blaha, P. (2009). Accurate Band Gaps of Semiconductors and Insulators with a Semilocal Exchange-Correlation Potential. *Physical Review Letters*, *102*(22), 226401. https://doi.org/10.1103/PhysRevLett.102.226401

Vogt, P., De Padova, P., Quaresima, C., Avila, J., Frantzeskakis, E., Asensio, M. C., Resta, A., Ealet, B., &

Le Lay, G. (2012). Silicene: Compelling Experimental Evidence for Graphenelike Two-Dimensional Silicon. *Physical Review Letters,* 108(15), 155501. https://doi.org/10.1103/PhysRevLett.108.155501

Wang, Q. H., Kalantar-Zadeh, K., Kis, A., Coleman, J. N., & Strano, M. S. (2012). Electronics and optoelectronics of two-dimensional transition metal dichalcogenides. *Nature Nanotechnology*, 7(11), 699-712. https://doi.org/10.1038/nnano.2012.193

Wei, Q., & Peng, X. (2014). Superior mechanical flexibility of phosphorene and few-layer black phosphorus. *Applied Physics Letters*, *104*(25), 251915. https://doi.org/10.1063/1.4885215

Zhang, J. L., Han, C., Hu, Z., Wang, L., Liu, L., Wee, A. T. S., & Chen, W. (2018). 2D Phosphorene: Epitaxial Growth and Interface Engineering for Electronic Devices. *Advanced Materials*, 30(47), 1802207. https://doi.org/10.1002/adma.201802207

Zhang, K., Feng, Y., Wang, F., Yang, Z., & Wang, J. (2017b). Two dimensional hexagonal boron nitride (2D-hBN): synthesis, properties and applications. *Journal of Materials Chemistry C*, *5*(46), 11992-12022. https://doi.org/10.1039/C7TC04300G

Zhang, X., Zhang, Z., Zhao, X., Wu, D., Zhang, X., & Zhou, Z. (2017a). Tetragonal-structured anisotropic 2D metal nitride monolayers and their halides with versatile promises in energy storage and conversion. *Journal of Materials Chemistry A*, *5*(6), 2870-2875. https://doi.org/10.1039/C6TA10980B